

# The Near Infrared Ca II Triplet as Metallicity Indicator: II Extension to extremely metal-poor metallicity regimes.\*

R. Carrera<sup>1,2†</sup> E. Pancino<sup>3,4</sup> C. Gallart<sup>1,2</sup> A. del Pino<sup>1,2</sup>

<sup>1</sup>*Instituto de Astrofísica de Canarias, La Laguna E-3200, Tenerife, Spain*

<sup>2</sup>*Departamento de Astrofísica, Universidad de La Laguna, La Laguna E-38205, Tenerife, Spain*

<sup>3</sup>*Osservatorio Astronomico di Bologna, via Ranzani 1, I-40127 Bologna, Italy*

<sup>4</sup>*ASI Science Data Center, I-00044 Frascati, Italy*

Accepted XXX. Received XXX; in original form XXX

## ABSTRACT

We extend our previous calibration of the infrared Ca II triplet as metallicity indicator to the metal-poor regime by including observations of 55 field stars with  $[\text{Fe}/\text{H}]$  down to  $-4.0$  dex. While we previously solved the saturation at high-metallicity using a combination of a Lorentzian plus a Gaussian to reproduce the line profiles, in this paper we address the non-linearity at low-metallicity following the suggestion of Starkenburg et al. (2010) of adding two non-linear terms to the relation among the  $[\text{Fe}/\text{H}]$ , luminosity, and strength of the Calcium triplet lines. Our calibration thus extends from  $-4.0$  to  $+0.5$  in metallicity and is presented using four different luminosity indicators:  $V-V_{HB}$ ,  $M_V$ ,  $M_I$ , and  $M_K$ . The calibration obtained in this paper results in a tight correlation between  $[\text{Fe}/\text{H}]$  abundances measured from high resolution spectra and  $[\text{Fe}/\text{H}]$  values derived from the CaT, over the whole metallicity range covered.

**Key words:** stars: abundances — stars: late-type —

## 1 INTRODUCTION

The infrared Ca II triplet (CaT) lines at 8498, 8542, and 8662 Å, easily differentiated even in low- and medium-resolution spectra ( $R \sim 2000$ – $10000$ ), are the main features of the near infrared spectra of late-type giant stars. Since their strengths change as a function of the metal content, they have been widely used as metallicity indicators in a variety of systems like open (e.g. Cole et al. 2004; Warren & Cole 2009; Carrera 2012) and globular (e.g. Armandroff & Zinn 1988; Rutledge et al. 1997b) clusters, dwarf spheroidal (e.g. Armandroff & Da Costa 1991; Pont et al. 2004; Battaglia et al. 2008) and irregular (e.g. Da Costa & Hatzidimitriou 1998; Tolstoy et al. 2001; Carrera et al. 2008b; Parisi et al. 2010) galaxies, and even in a more complex system like the Large Magellanic Cloud (e.g. Olszewski et al. 1991; Cole et al. 2005; Carrera et al. 2008a, 2011).

Initially, the CaT lines were employed to determine metallicities in relatively metal-poor and old systems such as the Galactic globular clusters (e.g. Armandroff & Zinn 1988; Armandroff & Da Costa 1991; Rutledge et al. 1997b). Most of these works utilized the classical approach of determining the equivalent widths of the CaT lines by fitting their profiles with Gaussian functions. The direct integration is hampered by the contamination of the wings with weak

neutral metal lines and molecular bands. There were some attempts of extending this calibration to more metal-rich and younger regimes. All of them were hindered by the non-Gaussian shape of damping wings in strong lines of stars with  $[\text{Fe}/\text{H}] > -1$  (e.g. Suntzeff et al. 1992, 1993; Rutledge et al. 1997b). To address this issue, Cole et al. (2004) proposed to fit the line profile with a sum of a Gaussian and a Lorentzian functions. For weak lines the Lorentzian component is equal to zero and the line profile is reproduced by a single Gaussian. In the case of strong lines, the Gaussian reproduces the line core but the Lorentzian component is necessary to properly sample the wings. Using this procedure Carrera et al. (2007, hereafter Paper I) extended the empirical calibration of the strength of the CaT lines as metallicity indicator for  $13 \leq \text{Age}(\text{Gyr}) \leq 0.25$  and  $-2.2 \leq [\text{Fe}/\text{H}] \leq +0.47$ . They also demonstrated that the age influence is negligible.

Curiously, none of the studies performed until that moment, and in particular those devoted to the metal-poor dwarf spheroidal galaxies, had detected stars more metal-poor than  $[\text{Fe}/\text{H}] \leq -3$  (e.g. Helmi et al. 2006). In contrast, the halo of the Milky Way contains a significant number of these objects which might reveal valuable information about the chemical evolution history of a galaxy, as they represent the most pristine (and probably thus the oldest) stars in the system. By comparison with metallicities derived from high-resolution spectroscopy analysis, Battaglia et al. (2008) found that CaT calibrations saturate for  $[\text{Fe}/\text{H}] \leq -2.5$ , and

† E-mail: rcarrera@iac.es

**Table 1.** Cluster sample.

Cluster	[Fe/H]	[Ca/H]	Ref.	[Fe/H] <sub>Paper I</sub>	Age(Gyr)	( <i>m</i> − <i>M</i> ) <sub>V</sub>	<i>E</i> ( <i>B</i> − <i>V</i> )	Ref.
NGC 104 (47 Tuc)	−0.76 ± 0.02	−0.45 ± 0.06	1,23	−0.67 ± 0.03	10.7 ± 1.0	13.32	0.05	8,13
NGC 188	−0.03 ± 0.04	−0.08 ± 0.03	2	−0.07 ± 0.04	6.30 ± 0.3	11.44	0.09	9,17
NGC 288	−1.32 ± 0.02	−0.90 ± 0.05	1,23	−1.07 ± 0.03	11.3 ± 1.1	14.64	0.03	8,13
NGC 362	−1.30 ± 0.04	−1.16 ± 0.05	1,28	−1.09 ± 0.03	8.7 ± 1.5	14.75	0.05	8,13
NGC 1851	−1.18 ± 0.08	−0.85 ± 0.03	1,25		9.2 ± 1.5	15.49	0.02	8,13
Berkeley 17	−0.10 ± 0.09	−0.15 ± 0.10	3		9 ± 0.5	14.27	0.61	27
NGC 1904 (M79)	−1.58 ± 0.02	−1.30 ± 0.04	1,23	−1.37 ± 0.05	11.7 ± 1.3	15.53	0.01	8,13
Berkeley 20	−0.30 ± 0.02	−0.22 ± 0.06	3	−0.49 ± 0.05	4.05 ± 0.7	15.84	0.38	9,22
NGC 2141	+0.00 ± 0.16	−0.11 ± 0.11	15	−0.14 ± 0.05	2.45 ± 0.9	14.15	0.40	9,14
Collinder 110	+0.03 ± 0.02	−0.04 ± 0.02	4		1.3 ± 0.2	13.04	0.40	24
NGC 2298	−1.96 ± 0.04	−1.52 ± 0.04	1,29	−1.74 ± 0.04	12.6 ± 1.4	15.54	0.13	8,13
Melotte 66	−0.33 ± 0.03	−0.22 ± 0.05	16	−0.38 ± 0.06	5.3 ± 1.4	13.63	0.14	9,26
Berkeley 39	−0.21 ± 0.01	−0.22 ± 0.07	19		7.0 ± 1.0	13.24	0.11	9,26
NGC 2682 (M 67)	+0.05 ± 0.02	−0.11 ± 0.03	4	−0.03 ± 0.03	4.3 ± 0.5	9.65	0.04	9,17
NGC 3201	−1.51 ± 0.02	−1.21 ± 0.07	1,23	−1.24 ± 0.12	11.3 ± 1.1	14.17	0.21	8,13
NGC 4590 (M 68)	−2.27 ± 0.04	−2.00 ± 0.04	1,23	−2.00 ± 0.03	11.2 ± 0.9	15.14	0.04	8,13
NGC 5927	−0.29 ± 0.07		1		10.9 ± 2.2	15.81	0.47	30,13
NGC 6352	−0.62 ± 0.05	−0.36 ± 0.07	1,31	−0.64 ± 0.02	9.9 ± 1.4	14.39	0.21	8,13
NGC 6528	+0.07 ± 0.08	+0.30 ± 0.08	1,32	−0.17 ± 0.02	11.2 ± 2.0	16.16	0.55	10,18
NGC 6681 (M 70)	−1.62 ± 0.08		1	−1.35 ± 0.03	11.5 ± 1.4	14.93	0.07	8,13
NGC 6705 (M 11)	+0.10 ± 0.07	−0.09 ± 0.06	5	+0.07 ± 0.05	0.25 ± 0.1	12.88	0.43	11
NGC 6791	+0.47 ± 0.07	+0.32 ± 0.08	6	+0.47 ± 0.04	12.0 ± 1.0	13.07	0.09	12
NGC 6819	+0.09 ± 0.03	+0.05 ± 0.06	7	+0.07 ± 0.03	2.9 ± 0.7	12.35	0.14	9,20,7
NGC 7078 (M 15)	−2.33 ± 0.02	−2.07 ± 0.10	1,23	−2.12 ± 0.04	11.7 ± 0.8	15.31	0.09	8,13
NGC 7789	+0.04 ± 0.07	−0.14 ± 0.09	4	−0.04 ± 0.05	1.3 ± 0.3	12.20	0.28	9,4,21

References: (1) Carretta et al. (2009a); (2) Jacobson et al. (2011); (3) Friel et al. (2005) (4) Pancino et al. (2010); (5) Gonzalez & Wallerstein (2000); (6) Carretta et al. (2007); (7) Bragaglia et al. (2001); (8) Salaris & Weiss (2002); (9) Salaris et al. (2004); (10) Feltzing & Johnson (2002); (11) Sung et al. (1999); (12) Stetson et al. (2003); (13) Rosenberg et al. (1999); (14) Carraro et al. (2001); (15) Jacobson et al. (2009); (16) Sestito et al. (2008); (17) Sarajedini et al. (1999); (18) Ortolani et al. (1992); (19) Friel et al. (2010); (20) Rosvick & Vandenberg (1998); (21) Gim et al. (1998); (22) Yong et al. (2005); (23) Carretta et al. (2010); (24) Bragaglia & Tosi (2003); (25) Carretta et al. (2011); (26) Kassis et al. (1997); (27) Bragaglia et al. (2006) (28) Shetrone & Keane (2000); (29) McWilliam et al. (1992); (30) Fullton (1996); (31) Feltzing et al. (2009); (32) Carretta et al. (2001).

therefore, they are not able to detect stars more metal-poor than this value.

It is well known that the strength of the CaT lines does not only depend on the metallicity but also on the temperature and gravity on the stellar surface. These contributions are removed using the fact that the strength of the CaT lines is linearly correlated with a luminosity indicator, used to trace the temperature and gravity variations, for stars in a range of 2-3 mag below the tip of the RGB for the metallicity range covered by open and globular clusters (e.g. Armandroff & Da Costa 1991; Rutledge et al. 1997a; Cole et al. 2004, Paper I). The calibration of the CaT lines as metallicity indicator is defined by the linear relation between the zero-point of these sequences and the metallicity. In Paper I it was noticed that the relation between the strength of the CaT lines and luminosity is not exactly linear if a larger luminosity range below the tip of the RGB is sampled. Recently, using synthetic spectra, Starkenburg et al. (2010) showed that, together with the fact that these sequences are not linear, the CaT saturation at lower metallicities is also due to the assumption of a linear relation between the zero-points of these sequences and metallicity. They obtained a new calibration with two additional terms to account for these issues.

However, this new calibration is based on synthetic spectra which suffer from uncertainties in the physics used to obtain them, particularly in this extremely metal-poor

regime. The goal of this paper is to study the behaviour of the CaT lines in extremely metal-poor stars ( $[\text{Fe}/\text{H}] \leq -2.5$ ) and obtain a new calibration of the strength of the CaT lines as metallicity indicator valid for the widest range of metallicities from observed spectra. To do that, the cluster sample used in Paper I has been complemented with observations of metal-poor field stars. Both samples are described in Section 2. The different luminosity indicators used are discussed in Section 3. The reference metallicities used are explained in Section 4. Section 5 accounts for the determination of the CaT lines equivalent widths and the CaT index definition. The new calibration of the CaT lines as metallicity indicator is obtained in Section 6, where it is also compared with other calibrations available in the literature. Finally, the main results of this paper are summarized in Section 7.

## 2 OBSERVATIONAL MATERIAL

### 2.1 Cluster sample

The CaT calibration obtained in paper I was obtained from observations of almost 500 RGB stars in 29 Galactic open and globular clusters, covering a total metallicity range of  $-2.33 \leq [\text{Fe}/\text{H}] \leq +0.47$ . We used the same sample in this paper, so we refer the reader to Paper I for a detailed discussion about the observations and data reduction of these stars. As in Paper I, Berkeley 32, NGC 2420, and NGC 2506 were

excluded from the analysis because of the small number of stars ( $\leq 5$ ) observed in each of them. Moreover, we excluded the globular cluster NGC 6715 (M54) with a well known intrinsic metallicity dispersion of  $\sim 0.19$  dex (e.g. Carretta et al. 2010). We have complemented the sample with observations of stars in the old and metal-rich open cluster Berkeley 17. This cluster was observed in November, 2005 with AF2/WYFFOS at the William Herschel Telescope (WHT) at the Roque de los Muchachos Observatory (La Palma, Spain) with the same setup used in Paper I (see table 2 of Paper I). The data reduction was performed and the radial velocities were calculated using IRAF<sup>1</sup> packages following the same procedure described in Paper I. Basically, after bias, overscan subtraction, and trimming, with *ccdproc*, dofibers were used to trace the apertures, make the flat-field correction, and perform the wavelength calibration. Finally, the sky lines were subtracted with a custom program (see Paper I for details). Eight of the observed stars have been confirmed as Berkeley 17 members from their radial velocity. From these stars we obtained a mean radial velocity of  $V_r = -79 \pm 11$  km s<sup>-1</sup> in good agreement, within the uncertainties, with other values available in the literature:  $-84 \pm 11$  km s<sup>-1</sup> (Friel et al. 2002), and  $-73.7 \pm 0.8$  km s<sup>-1</sup> (Friel et al. 2005). The final sample includes stars of 25 clusters which are listed in Table 1 together with the main characteristics and the reference metallicities for each of them.

## 2.2 Metal-poor stars

Unfortunately there are no clusters more metal-poor than  $[\text{Fe}/\text{H}] \sim -2.3$  dex. Therefore, to investigate the behavior of the CaT lines at lower metallicity we have complemented the cluster sample with observations of metal-poor field stars. These stars were observed in two runs in April 2011 and February 2012 with IDS at the Issac Newton Telescope (INT) located at the Roque de los Muchachos Observatory (La Palma, Spain). The instrument configuration used is described in detail in Carrera (2012). The exposure times were selected as a function of the magnitude of the stars in order to ensure a signal-to-noise ratio (S/N) greater than 20. Observed stars, together with the S/N, and magnitudes in V bandpass are listed in Table 2. The data reduction was performed in the same way as in Paper I for the cluster stars using IRAF packages. Several cluster stars previously studied in Paper I and a field metal-rich object, HD15656 ( $[\text{Fe}/\text{H}] = -0.16$ ), were also observed in both runs to ensure the homogeneity of the sample. The differences between the equivalent widths obtained in each run are  $\sim 0.1$  Å, which is similar to the mean uncertainty in the equivalent width determination itself (see Section 5). The radial velocity of each star was calculated using the *fxcor* task in IRAF using as template some of the stars with the best S/N in our sample. The final radial velocity for each target star was obtained as the average of the velocities obtained for each template,

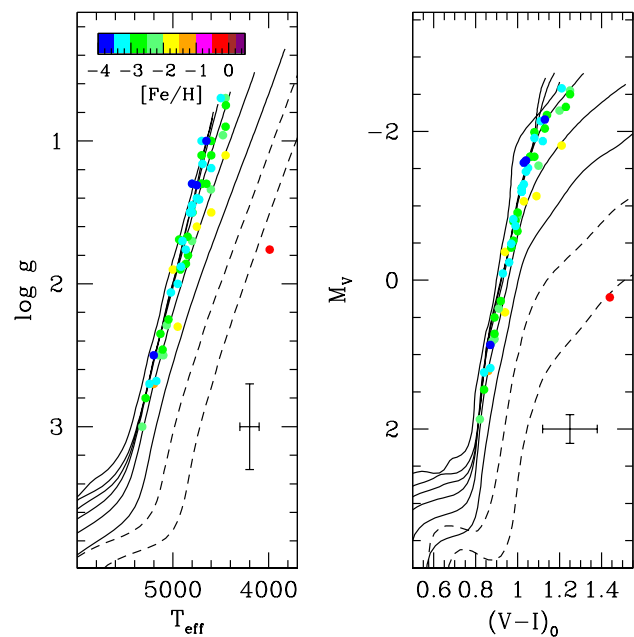


**Figure 1.** Location of the observed metal-poor stars in the  $T_{\text{eff}}$ - $\log g$  (left) and  $(V-I)_0$ - $M_V$  (right) planes. Each star has been coloured as a function of its metallicity. Overplotted are the Y<sup>2</sup> (Yale-Yonsei) isochrones: solid lines are 10 Gyr old isochrones of  $[\alpha/\text{Fe}] = +0.6$  and  $-4.0 \leq [\text{Fe}/\text{H}] \leq -1.5$  with a step of 0.5 dex; dashed lines are 8 Gyr old isochrones with  $[\alpha/\text{Fe}] = +0.0$  and  $[\text{Fe}/\text{H}] = -0.5$  and 0.0. Typical errorbars are plotted in bottom-right corner of each panel.

weighted by the width of the correlation peaks. The measured radial velocity for each star are listed in Table 2.

## 3 LUMINOSITY INDICATOR

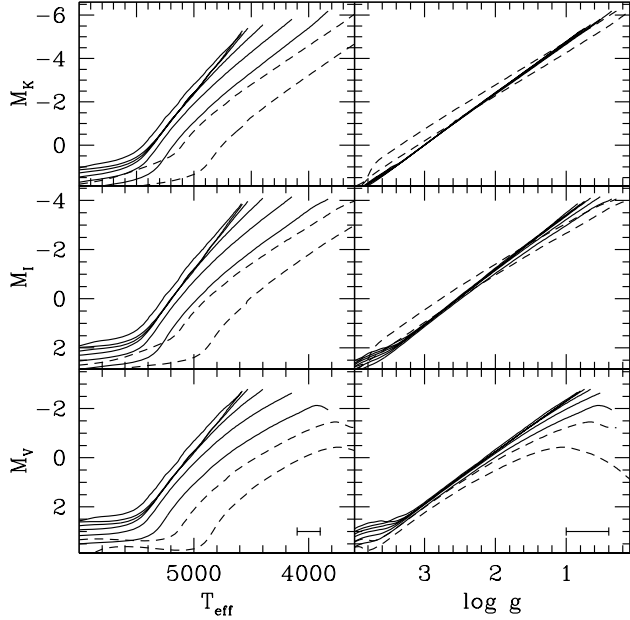
Several luminosity indicators have been used in the literature to remove the temperature and gravity contributions and leave only the abundance dependence in the CaT line strengths. The magnitude of a star relative to the position of the horizontal branch (HB) in the V filter, denoted as  $V - V_{\text{HB}}$ , is the most used one (e.g. Armandroff & Da Costa 1991; Rutledge et al. 1997b; Cole et al. 2004). Although it also removes any dependence on distance and reddening, it is hampered by the difficulty of defining the HB position in field stars, poorly populated clusters or galaxies with extended star formation histories. While in the case of old metal-poor systems, like globular clusters, the magnitude of the HB is defined as the RR Lyrae instability strip position, the red clump (RC) location has been used in the case of young metal-rich objects like open clusters. Some authors tried to account for this difference (e.g. Da Costa & Hatzidimitriou 1998) whereas others omit it (e.g. Cole et al. 2004). In the case of galaxies it is not possible to do this correction without an initial indication of the age of the stars. For example in a galaxy with multiple star formation epochs like the Large Magellanic Cloud, the difference between the position of the RR Lyrae instability strip and the median magnitude of the RC can be as large as 0.4 mag. Since it is not possible to estimate the age of a given star prior to

<sup>1</sup> Image Reduction and Analysis Facility, IRAF is distributed by the National Optical Astronomy Observatories, which are operated by the Association of Universities for Research in Astronomy, Inc., under cooperative agreement with the National Science Foundation.

**Table 2.** Metal-poor star sample. The full version of this table is available in the online journal and in the CDS.

Star	$T_{eff}$	$\log g$	[Fe/H]	[Ca/H]	Ref.	V	$M_V$	$M_I$	$M_K$	$V_r$ (km s <sup>-1</sup> )	S/N
CS31082-0001	4922±100	1.9±0.3	-2.78±0.19	-2.62±0.24	1	11.32	-0.51±0.13	-1.48±0.14	-2.71±0.16	139±3	73.0
CS22175-0007	5108±100	2.5±0.4	-2.81±0.18	-2.50±0.23	1	13.49	0.64±0.13	-0.25±0.13	-1.42±0.14	-5±5	55.0
HD15656	3990±100	1.8±0.3	-0.16±0.17	-0.25±0.20	6	5.16	0.18±0.10	-1.25±0.10	-2.98±0.09	-47±6	140.0

References: (1) Barklem et al. (2005); (2) Andrievsky et al. (2011); (3) Lai et al. (2008) (4) Johnson (2002); (5) McWilliam (1990); (6) Hollek et al. (2011); (7) Fulbright (2000); (8) Wu et al. (2011); (9) Luck & Bond (1985); (10) Pilachowski et al. (1996); (11) McWilliam et al. (1995); (12) Giridhar et al. (2001); (13) Zhang et al. (2009).

**Figure 2.** Behaviour of  $T_{eff}$  (left) and  $\log g$  (right) as a function of  $M_V$  (bottom),  $M_I$  (middle), and  $M_K$  (top) for the same isochrones used in Fig. 1.

the measurement of its metallicity, this implies a metallicity uncertainty as large as  $\sim 0.15$  dex.

Alternatively, other authors used the absolute magnitude in the  $V$  and/or  $I$  Johnson-Cousins bandpasses (e.g. Pont et al. 2004; Carrera et al. 2008a,b, 2011). Moreover in the case of external galaxies, the absolute magnitudes, which are obtained from distance and reddening, are often known with an accuracy better than 0.4 mag. In any case, determining stellar metallicities from CaT lines in the closed galaxies is usually hindered by the need of homogeneous photometry samples covering wide areas. Recently, Warren & Cole (2009) and Saviane et al. (2012) proposed to use the absolute magnitude in the  $K_S$  bandpass. The Two Micron All-Sky Survey (2MASS; Skrutskie et al. 2006) provides homogeneous photometry in near-infrared  $J$ ,  $H$ , and  $K_S$  bandpasses for almost the whole celestial sphere with an accuracy better than 0.03 mag and an astrometric precision of about 0.1 arcsec. Since the magnitude limit of 2MASS in  $K_S$  band is 14.3, this implies that this survey has sampled the brightest RGB stars in almost all satellites of the Milky Way including the Magellanic Clouds. In order to obtain a calibration as general as possible, we have used as luminosity indicators both the absolute magnitude in the  $V$ ,  $I$ , and  $K_S$

bandpasses and the magnitude relative to the HB position in the  $V$  filter.

The absolute and relative magnitudes of cluster stars have been obtained from the distance modulus, reddening, and HB positions listed in Table 1. The reference photometry in  $V$  and  $I$  for each cluster was described in Paper I. In the case of Berkeley 17 the magnitudes of observed stars have been obtained from Bragaglia et al. (2006). The HB position of globular clusters were obtained from the updated version of the Harris globular cluster database<sup>2</sup> (Harris 1996). In the case of open clusters, the HB/RC position has been obtained from the original references of the photometry of each cluster (see Paper I) and from Cole et al. (2004).

Unfortunately, the absolute magnitudes of the field stars in our sample are unknown. To derive them we followed a similar procedure to that described by Breddels et al. (2010). It consists on calculating the absolute magnitudes from observable quantities using theoretical stellar evolution models. In our case, we used as input observable parameters the effective temperature ( $T_{eff}$ ), surface gravity ( $\log g$ ), and metallicity ([Fe/H]), derived from high-resolution spectroscopy. Because they properly sample the extremely metal-poor regimes of our field star sample we assumed the  $Y^2$  Yonsei-Yale stellar evolution models (Demarque et al. 2004) available at <http://www.astro.yale.edu/demarque/yyiso.html>. Using the *YYmix2* interpolation routine provided together with the  $Y^2$  models we created a grid of isochrones for  $-4.0 \leq [\text{Fe}/\text{H}] \leq 0.0$  with a separation of 0.5 dex,  $2 \leq \text{Age} \leq 12$  Gyr with a step of 2 Gyr, and three different  $\alpha$ -elements abundances:  $[\alpha/\text{Fe}] = 0.0, +0.3, \text{ and } +0.6$  dex.

In the left panel of Fig. 1 a sample of isochrones of different metallicities have been plotted in the  $T_{eff}$ - $\log g$  plane. The field stars in our sample have been overplotted with different colours, as a function of their metallicities. Since isochrones for certain ranges of ages and metallicities overlap it is not possible to infer unique age and metallicity, and therefore, they may imply uncertainties in the derived absolute magnitudes. For this reason we use a statistical approach which provides a probability distribution for each recovered magnitude.

In addition, the uncertainties of the input parameters affect the derived magnitudes. Typical errorbars for  $T_{eff}$  and  $\log g$  are also plotted in bottom-right corner of left panel in Fig. 1. Breddels et al. (2010) presented a detailed discussion about how  $T_{eff}$  and  $\log g$  uncertainties affect the recovered absolute magnitudes for both main-sequence and RGB

<sup>2</sup> <http://physwww.physics.mcmaster.ca/harris/mwgc.dat>

stars. In our case we limited our discussion to RGB objects. In Fig. 2 we have plotted the same isochrones as in Fig. 1 illustrating the relations between  $T_{eff}$  and  $\log g$  with  $M_V$ ,  $M_I$ , and  $M_K$  to investigate the impact of the uncertainties in the derived absolute magnitudes. It is clear that for RGB stars the absolute magnitudes are better constrained by  $\log g$  than by  $T_{eff}$ . Therefore a large  $\log g$  error implies a large uncertainty in the determination of  $M_V$ ,  $M_I$ , and  $M_K$ . For example, a  $\sigma_{\log g}$  of about  $\pm 0.3$  dex for a star with  $\log g = 1.5$  dex implies uncertainties of  $\pm 0.5$ ,  $0.6$ , and  $0.65$  mag for  $M_V$ ,  $M_I$ , and  $M_K$ , respectively using a 8 Gyr old isochrone with  $[\text{Fe}/\text{H}] = -2.0$  dex, and  $[\alpha/\text{Fe}] = +0.6$  dex. In the same way, a  $\sigma_{T_{eff}}$  of about  $\pm 100$  K for a star of  $T_{eff} = 4500$  K implies uncertainties of  $\pm 0.3$ ,  $0.35$ , and  $0.4$  mag for  $M_V$ ,  $M_I$ , and  $M_K$ , respectively. Assuming different ages produces similar uncertainties as changing the temperature. Lower uncertainties are produced by the errors in  $[\text{Fe}/\text{H}]$  and  $[\alpha/\text{Fe}]$  ratios as was demonstrated by Breddels et al. (2010). For this reason, the  $[\alpha/\text{Fe}]$  ratio was not used as input parameter.

In order to match the observational input parameters with the absolute magnitudes provided by stellar evolution models we perform a classical  $\chi^2$  minimisation defined as:

$$\chi^2 = \sum_{i=0}^{n=3} \frac{(A_i - A_{i,model})^2}{\sigma_{A_i}^2} \quad (1)$$

where  $A_i$  are the three observable atmosphere parameters and  $A_{i,model}$  the corresponding parameters of the model, as given by the set of isochrones.  $\sigma_{A_i}$  represent the uncertainties of the observational quantities used as input. Although we used the specific uncertainties for each star, on average  $\sigma_{T_{eff}}$  is  $\sim 100$  K,  $\sigma_{\log g}$  is  $\sim 0.25$  dex, and  $\sigma_{[\text{Fe}/\text{H}]}$  is  $\sim 0.1$  dex.

To take into account the impact of the input parameter uncertainties on the derived magnitudes, we performed a Monte Carlo realisation. For each star we computed 5000 fakes stochastically varying the input parameters, assuming that each of them behaves as a Gaussian probability distribution which mean and sigma are the given value and its uncertainty. Each fake is compared with each model point in the isochrone grid using Equation 1. Instead of considering only the best solution, we adopted as absolute magnitudes for each fake the average of the values provided by the 20 best matches since different combinations of the input parameters can produce very similar  $\chi^2$  values. The absolute magnitudes of the 5000 fakes for each star are Gaussianly distributed and therefore, we adopted as the absolute magnitude and its uncertainty the mean and sigma of each distribution. The obtained values and their uncertainties are listed in Table 2 and have been plotted in the right panel of Fig. 1. In general, the obtained magnitudes have uncertainties lower  $\sim 0.2$  mag.

In order to check the reliability of this method we have applied it to stars in four clusters: NGC 104, NGC 4590, NGC 7078, and Berkeley 39. They have been selected to sample a wide range of metallicities and in particular the metallicity range in which both field and cluster samples overlap around  $[\text{Fe}/\text{H}] \sim -2$  dex. Therefore, this test also is valid to ensure that there is no bias between the two samples. For the three globular clusters we consider the red giant stars observed with high-resolution spectroscopy by Carretta et al. (2009b) who determined temperatures, surface gravities,

and metallicities for more than 50 stars in each system. In the same way, we use the red giant stars analysed by Bragaglia et al. (2012) in the open cluster Berkeley 39. The  $I$  magnitudes of the globular clusters stars have been selected from the SUMO project (Monelli et al. 2013) since Carretta et al. (2009b) do not provide them. We have used the method described above to estimate the absolute magnitudes from the temperature, surface gravity and metallicity. Obtained values have been compared with the absolute magnitudes derived from the distance modulus and reddening listed in Table 1 as was done for cluster stars. We find that the differences between the values derived from the two procedures are on average  $-0.11 \pm 0.09$ ,  $-0.12 \pm 0.09$ , and  $-0.12 \pm 0.12$  for  $M_V$ ,  $M_I$ , and  $M_K$ , respectively. These values are of the same order of the typical uncertainties of the absolute magnitudes derived from the method used for field stars. We conclude that our procedure provides reliable magnitudes within the uncertainties. This result also ensures that there is no significant bias between the absolute magnitudes derived for cluster and field stars.

Finally, to use  $V - V_{HB}$  as luminosity indicator we have to define the HB position for each field star. Unfortunately, there is no much information about the position of the HB at extremely metal-poor regimes. Starkenburg et al. (2010) estimated the position of HB from the empirical  $M_V$ - $[\text{Fe}/\text{H}]$  relationship ( $M_{V,HB} = 0.23 \times [\text{Fe}/\text{H}] + 0.931$ ) obtained by Catelan & Cortés (2008). However, this relationship was obtained in the metallicity range covered by Galactic globular clusters and therefore, for  $[\text{Fe}/\text{H}] \geq -2.25$  (see Catelan & Cortés 2008, and references therein). To our knowledge, there is neither theoretical nor empirical better estimations of the position of the HB for more metal-poor regimes. For this reason, we also used this relationship to estimate the position of the HB for our field star sample although its extrapolation to these regimes should be taken with care.

## 4 REFERENCE METALLICITIES

Another important point to obtain the calibration of the CaT lines as metallicity indicator is the reference metallicity scale used. Unfortunately, there is no scale which includes clusters, both open and globular, and field stars. In fact there is even no common metallicity scale for open and globular clusters. For this reason the reference metallicities have been chosen from different sources as is explained below. Any attempt to homogenize them is clearly beyond the scope of this paper.

In the literature, we can find three metallicity scales for globular clusters. The traditional Zinn & West (1984) metallicity scale derived from low-resolution spectra and two more obtained from high-resolution spectra ( $R > 20000$ ): Kraft & Ivans (2003) and Carretta et al. (2009a), which is the updated version of Carretta & Gratton (1997). There are systematic differences among these three scales due to the resolution of the spectra, lines used for the analysis, etc. The different authors offer comparisons among them that can be used to switch from one scale to another. Because of the large number of clusters studied and the number of stars analysed in each of them we have chosen the Carretta et al. (2009a) metallicities as the reference for the globular clusters in our sample. It is also important that in this work, the

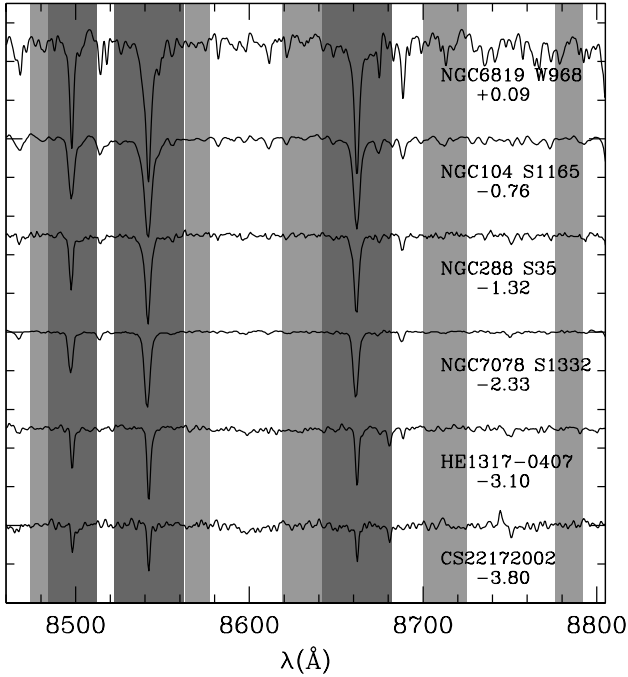


**Figure 3.** Continuum (clear) and line (dark) bandpasses defined by Cenarro et al. (2001) overplotted onto stars of different metallicities.

[Fe/H] abundances were obtained using both Fe I and Fe II spectral lines.

In the case of open clusters, several teams are working in deriving metallicities, and abundances of other chemical species, in an homogeneous way. Unfortunately, none of them include all the systems in our sample (see Carrera & Pancino 2011, for a recent compilation of open clusters metallicities). For this reason, we have chosen the reference metallicities of open clusters from different sources, with the constraint that they have to be derived from spectra of resolution equal or larger than 20000 and using both Fe I and Fe II spectral lines. These criteria have been also used to select the reference metallicities of the field stars in our sample. Moreover, the average metallicity of each open cluster must have been obtained from at least three stars. The reference metallicities used for cluster and field stars are listed in Tables 1 and 2, respectively.

## 5 THE CAT INDEX

The strength of each CaT line was obtained in the classical way by determining the area between the spectral line inside a bandpass covering the feature, and the continuum level calculated in several bandpasses among the three CaT lines. Although several definitions of these bandpasses can be found in the literature (see Paper I for a comparison), in Paper I we selected those defined by Cenarro et al. (2001). The line bandpasses are defined to cover completely each spectral line and in particular the wings of strong metal-rich lines. The continuum bandpasses are selected to avoid the presence of other spectral lines and molecular bands. In Fig. 3 we have overplotted the Cenarro et al. (2001) bandpasses onto stars of different metallicities. The selected bandpasses sample

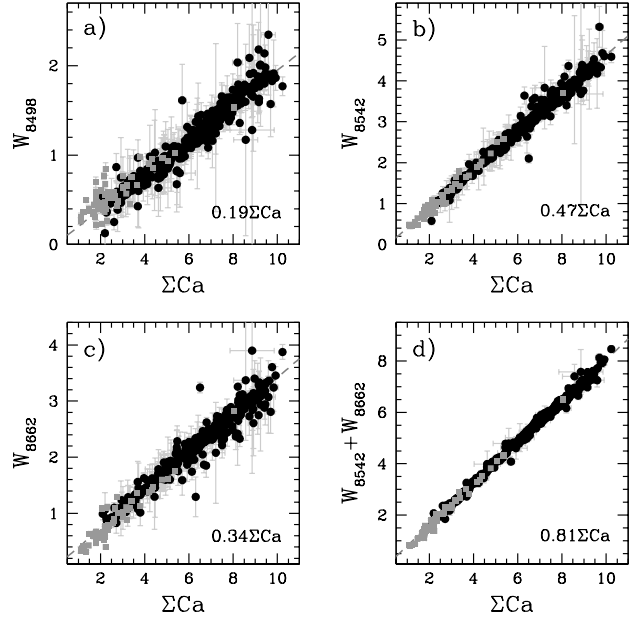


**Figure 4.** Run of the strength of each individual CaT line versus the  $\Sigma Ca$  index for both clusters (black) and metal-poor stars (grey), obtained as the sum of the equivalent widths of the three lines. The run of the sum of the equivalent widths of the two strongest lines versus  $\Sigma Ca$  is also plotted. The fractional contribution of each line or combination, to the total  $\Sigma Ca$  is labelled.

**Table 3.** Equivalent widths of the three CaT lines for both cluster and field stars in our sample. The full version of this table is available in the online journal and in the CDS.

ID	$W_{8998}$	$W_{8542}$	$W_{8662}$
NGC 104 L2705	$1.33 \pm 0.02$	$3.21 \pm 0.03$	$2.73 \pm 0.03$
NGC 104 L2707	$1.33 \pm 0.07$	$3.17 \pm 0.10$	$2.45 \pm 0.09$
NGC 104 L2720	$1.25 \pm 0.12$	$2.96 \pm 0.13$	$2.30 \pm 0.12$
BD+053098	$0.52 \pm 0.02$	$1.21 \pm 0.02$	$0.82 \pm 0.02$
BD-185550	$0.46 \pm 0.02$	$0.78 \pm 0.03$	$0.61 \pm 0.03$
BD+233130	$0.40 \pm 0.03$	$0.77 \pm 0.04$	$1.09 \pm 0.03$

properly both metal-poor weak and metal-rich strong lines. Moreover, continuum bandpasses are not strongly affected by molecular bands in both metal-poor and metal-rich stars.

The profile of each CaT line is fitted by a combination of a Gaussian plus a Lorentzian. As was described in Paper I, this combination provides the best fit to the line core and wings for both weak and strong lines. The fit is also good for the very weak lines of extremely metal-poor stars. This least square fit was performed using the Levenberg-Marquadt algorithm. Although in our case the spectra had already been normalized, the position of the continuum was recalculated by performing a linear fitting to the mean values of each continuum bandpass. Finally, the equivalent width is obtained as the area delimited by the profile fitted to the line and the continuum level. The equivalent widths of each CaT line and their uncertainties determined for both field and cluster stars are listed in Table 3.

Different ways of combining the strengths of the three CaT lines can be found in the literature in order to obtain the global CaT index,  $\Sigma Ca$  (see Cenarro et al. 2001,

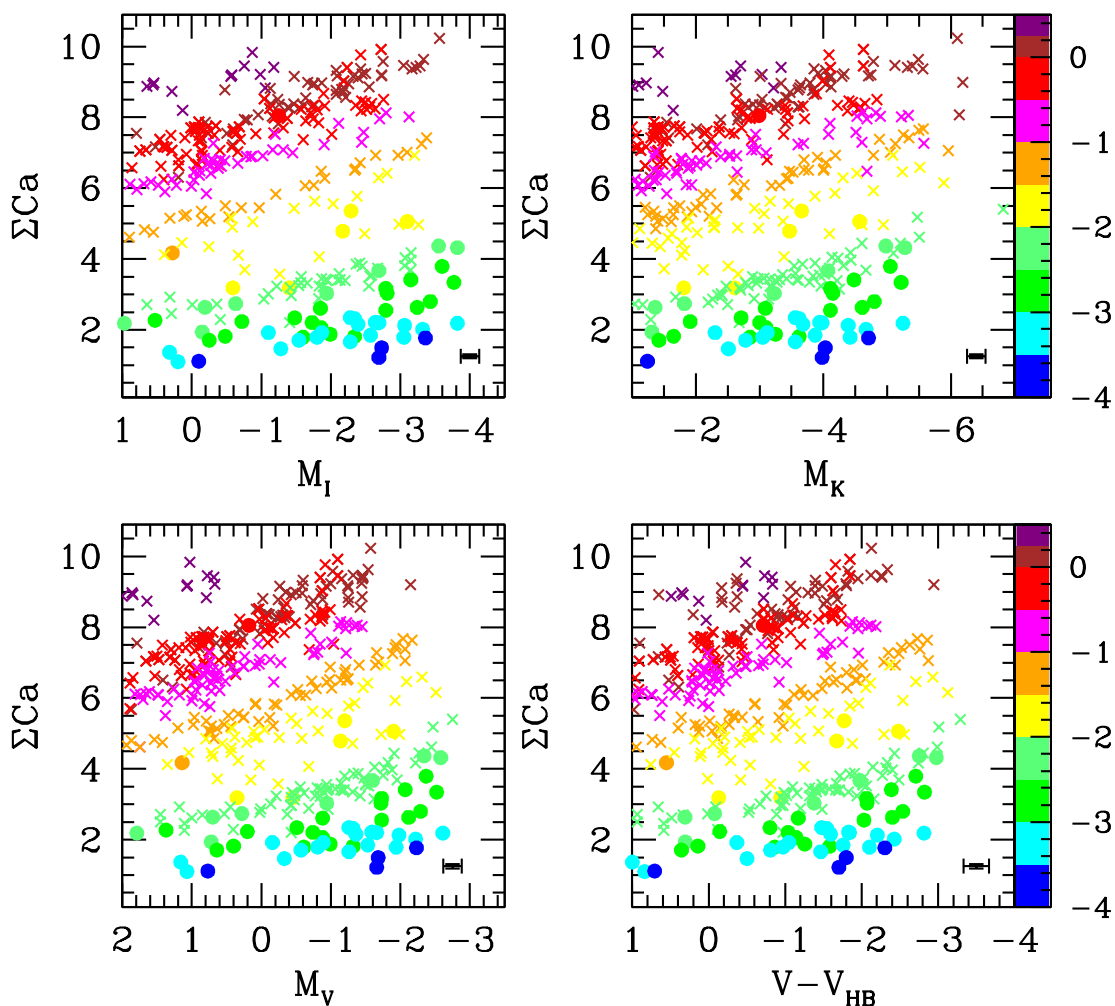


**Figure 5.** Run of  $\Sigma Ca$  as a function of  $M_V$ ,  $V - V_{HB}$ ,  $M_I$ , and  $M_K$ . Stars of different  $[Fe/H]$  have been plotted with different colors. Crosses and filled circles represent cluster and field stars, respectively. Error bars in bottom-right corner of each panel show the mean uncertainties.

for a comparison among different index definitions). The most used ones are the unweighted sum of the three features,  $W_{8498} + W_{8542} + W_{8662}$  (e.g. Cole et al. 2004, Paper I), or the unweighted sum of the two strongest lines,  $W_{8542} + W_{8662}$  (e.g. Suntzeff et al. 1993; Battaglia et al. 2008). In the last one, the weakest line at 8498 Å is excluded on the basis of its worse S/N. In Fig. 4 we have plotted the run of  $\Sigma Ca$ , obtained as the sum of the equivalent widths of the three CaT lines, versus the equivalent width of each CaT feature (panels a, b and c respectively) and the sum of the two strongest lines (panel d). In all cases a clear linear correlation is observed. The contribution of the weakest line at 8498 Å to  $\Sigma Ca$  is only the 19%. The other two lines at 8542 and 8662 Å contribute with the 47% and 34%, respectively. Although we obtain our calibration as a function of  $\Sigma Ca$ , these relations allow to transform it to any other combination of the strength of the three CaT lines. We also investigated the ratio between the strength of the two strongest CaT lines. For all the stars in our sample we obtained  $W_{8542}/W_{8662} = 1.32 \pm 0.09$  without any dependence in absolute magnitude. Although

within the dispersion, there is a small trend with metallicity in the sense that the ratio decreases with metallicity ( $W_{8542}/W_{8662} = 1.36 + 0.04 \times [Fe/H]$ . Starkenburg et al. (2010) derived a mean ratio of 1.27 in their synthetic spectra. They also found a similar dependence with metallicity in their synthetic spectra. Norris et al. (2008) obtained a ratio of 1.34 in globular cluster stars. Anyway, all these values are similar within the errorbars.

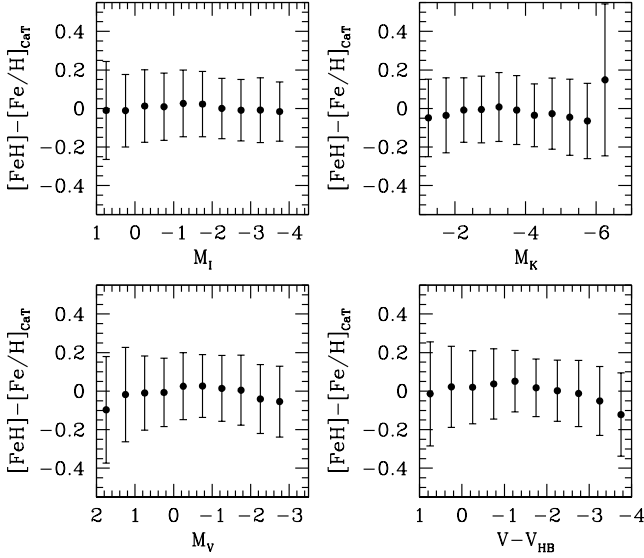
## 6 THE CA II TRIPLET METALLICITY SCALE

### 6.1 A new CaT calibration valid for $-4 \leq [Fe/H] \leq +0.5$

As explained above, the calibration of the CaT lines as metallicity indicator traditionally relies on the fact that stars of a given metallicity describe a linear sequence in the  $\Sigma Ca$ -Luminosity plane. Since the slope was supposed to be independent of metallicity, the variation of the zero-points with metallicity define the CaT calibration. This approximation fails for large luminosity ranges in the RGB (Paper I) and in

**Table 4.** Best fitting parameters

	$V$	$V - V_{HB}$	$I$	$K_S$
a	$-3.45 \pm 0.04$	$-3.45 \pm 0.04$	$-3.43 \pm 0.04$	$-3.33 \pm 0.05$
b	$0.16 \pm 0.01$	$0.11 \pm 0.02$	$0.13 \pm 0.01$	$0.15 \pm 0.01$
c	$0.41 \pm 0.004$	$0.44 \pm 0.006$	$0.45 \pm 0.006$	$0.48 \pm 0.008$
d	$-0.53 \pm 0.11$	$-0.65 \pm 0.12$	$-0.50 \pm 0.12$	$-0.27 \pm 0.13$
e	$0.019 \pm 0.002$	$0.03 \pm 0.003$	$0.016 \pm 0.002$	$0.01 \pm 0.002$
$\sigma$	0.17	0.16	0.16	0.17
N	422	401	321	413

**Figure 6.** Mean and sigma of the difference between the reference metallicities and those obtained from Equation 2 for each luminosity indicator.

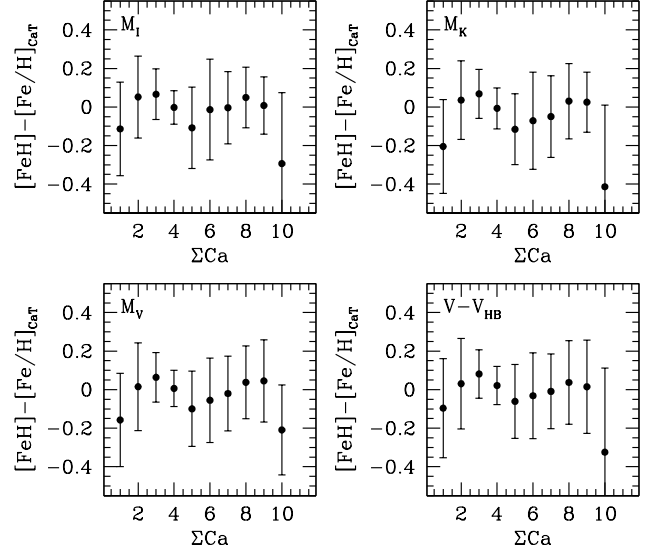
particularly for extremely metal-poor stars (Starkenburg et al. 2010). Moreover, Starkenburg et al. (2010) noted that the zero-points of these sequences do not change linearly with metallicity as was assumed until that moment.

The run of  $\Sigma Ca$  versus  $M_I$ ,  $M_K$ ,  $M_V$ , and  $V - V_{HB}$  for the stars in our sample is shown in Fig. 5. Stars of different metallicities have been plotted with different colors. From this figure, it is clearly noticed that the slopes and the shape of the sequences change as a function of metallicity for all four luminosity indicators used. This is more clear in the extremely metal-poor regime. The change of the shape of the sequences as a function of metallicity is also clearly noticed. To address these effects, Starkenburg et al. (2010) proposed to add two new terms to the relationship used to obtain the CaT calibration: a cross term to account for the slope changes as a function of  $[Fe/H]$ , and a term of  $\Sigma Ca^{-1.5}$  to account for the changing offset. We have used the same analytic relationship to derive our calibration which is in the form:

$$[Fe/H] = a + b \times Mag + c \times \Sigma Ca + d \times \Sigma Ca^{-1.5} + e \times \Sigma Ca \times Mag \quad (2)$$

where  $Mag$  refers to each luminosity indicator.

The values obtained for the terms  $a$ ,  $b$ ,  $c$ ,  $d$ , and  $e$  for each luminosity indicator are listed in Table 4 together with the number of stars used in each case and the sigma of the fit.

**Figure 7.** As Fig. 6 but as a function of  $\Sigma Ca$ .

The uncertainties of each parameter obtained by the normal least squares fit are very small. To compute more realistic uncertainties for each term we performed a Monte Carlo realisation. The input values of each star are randomly varied within their uncertainties assuming that they behave as a Gaussian probability distribution. A least square fit is performed using the modified input values. This procedure is repeated 5000 times. As expected, the values obtained as the mean of the results of each realisation are the same that those obtained by the original least square fit. The dispersion of these values provides a more realistic estimation of the uncertainty of each term which are also listed in Table 4. We have tested if the quality of the fit improve by changing the term  $\Sigma Ca^{-1.5}$  for  $\Sigma Ca^2$ . However, the goodness of the fit worsens if the  $\Sigma Ca^2$  term is used. We also investigated if the sigma of the fit decreases by adding quadratic terms. We found that adding new terms does not improve significantly the quality of the fit.

The mean and sigma of the residuals of the fit as a function of each luminosity indicator have been plotted in Fig. 6 and Fig. 7. Since there is not clear tendency neither with the position along the RGB nor with  $\Sigma Ca$ , and therefore with  $[Fe/H]$  we conclude that our calibration performs well for the whole range of metallicities studied. In general, the scatter of the residuals are above  $\sim 0.15$  dex which is slightly lower than the typical error bar of the  $[Fe/H]$  values derived from CaT calibrations which is  $\sim 0.15$ – $0.20$  dex.

## 6.2 Comparison with other calibrations

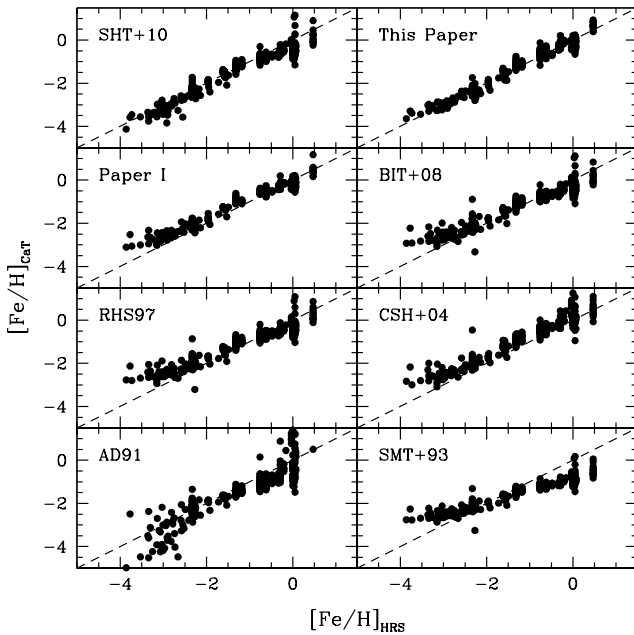
Several comparisons among the different CaT indices can be found in the literature using stars in common among different studies (Rutledge et al. 1997b, Paper I). However, to our knowledge, only Battaglia et al. (2008) compared the final metallicities derived from their CaT calibration with reference values derived independently from high-resolution spectroscopy. It would be very useful to compare the metallicities derived from the different CaT calibrations available in the literature with the reference values obtained from the



**Table 5.** Compilation of the main features of the different CaT calibrations compared in this work.

Source	$\Sigma Ca$	Luminosity	Line fitting	Bandpasses
AD91	$W_{8542} + W_{8662}$	$V - V_{HB}$	Gaussian	AD91
SMT+93	$W_{8542} + W_{8662}$	$V - V_{HB}$	Gaussian	AZ88
RHS97	$0.5W_{8498} + W_{8542} + 0.6W_{8662}$	$V - V_{HB}$	Moffat	RHS97
CSH+04	$W_{8498} + W_{8542} + W_{8662}$	$V - V_{HB}$	Gaussian+Lorentzian	AZ88
Paper I	$W_{8498} + W_{8542} + W_{8662}$	$M_I$	Gaussian+Lorentzian	CCG+01
BIT+08	$W_{8542} + W_{8662}$	$V - V_{HB}$	Gaussian	BIT+08
SHT+10	$W_{8542} + W_{8662}$	$V - V_{HB}$	Gaussian	BIT+08
This Paper	$W_{8498} + W_{8542} + W_{8662}$	$M_I$	Gaussian+Lorentzian	CCG+01

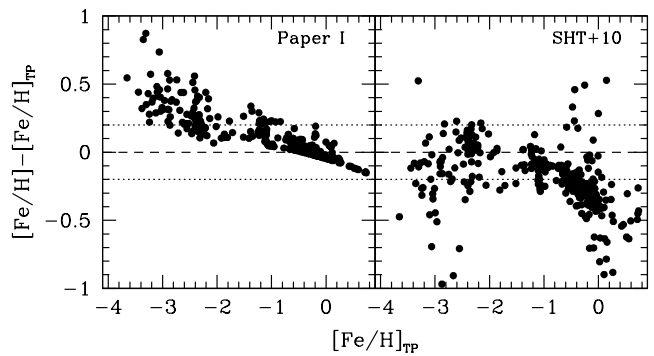
References: AZ88: Armandroff & Zinn (1988); AD91: Armandroff & Da Costa (1991); SMT+93: Suntzeff et al. (1993); RHS97: Rutledge et al. (1997a,b); CCG+01: Cenarro et al. (2001); BIT+08: Battaglia et al. (2008); SHT+10: Starkenburg et al. (2010).


**Figure 8.** Comparison among different CaT calibrations available in the literature and reference metallicities (see text and Table 5 for details).

analysis of both Fe I and Fe II spectral lines in high-resolution spectra. The CaT calibrations are based on four ingredients: the bandpasses used to determine the continuum and spectral features; the way in which the line profile is fit; the reference metallicities used; and the form of the relationship among the CaT index, the luminosity indicator and the reference metallicities. In Section 1, it has been explained in detail how different assumptions on some of these points affect the final CaT calibration.

We have selected eight reference works which are listed in Table 5, together with the different approach used by each of them. They have been selected in order to include the most used bandpasses, line profile functions and relationships among CaT index, luminosity indicator and metallicity.

To perform this comparison we have determined the equivalent width of each CaT line in the same clusters and metal-poor stars used in this paper. We have followed the procedure that define each calibration, i.e. used the same bandpasses, line profile functions, index definitions, lumi-


**Figure 9.** Differences of the metallicities obtained by the calibration derived in Paper I (left) and those calculated with the relationship derived by Starkenburg et al. (2010, right) with the values computed with the new calibration derived in this paper. Dotted lines represent a typical uncertainty of  $\pm 0.2$  dex.

nosity indicators and relationships among CaT index, luminosity indicator and reference metallicities. We refer the reader to the original papers for a detailed description of each procedure.

In Fig. 8 we have plotted the high-resolution reference metallicities (X-axis) described in Section 4 versus the metallicity values obtained with each calibration (Y-axis). The Armandroff & Da Costa (1991) calibration has the largest scatter, particularly at the metal-poor regime. This may be explained by the fact that it is the only one in which a quadratic relationship has been assumed between the reduced equivalent widths and metallicities. However, it behaves well in the metallicity range in which it was defined ( $-2 \leq [Fe/H] \leq -0.7$ ). All the calibrations before Starkenburg et al. (2010), including that obtained in Paper I, saturate at extremely metal-poor regimes ( $[Fe/H] \leq -2.5$ ) as was noted by Battaglia et al. (2008). A large scatter is observed at metal-rich regimes ( $[Fe/H] \geq -0.25$ ) with the exception of the one obtained in Paper I. These is observed even in the case of the one derived by Cole et al. (2004) which used metal-rich open clusters as calibrators, together with metal-poor globular clusters. This denotes that together with the inclusion of the Lorentzian profile to sample the strong wings in metal-rich stars as was proposed by Cole et al. (2004), it is key to use bandpasses large enough to sample completely the wings of strong lines. The addition of two new terms in the relationship among the CaT index, luminosity indicator and metallicity proposed by Starkenburg et al.

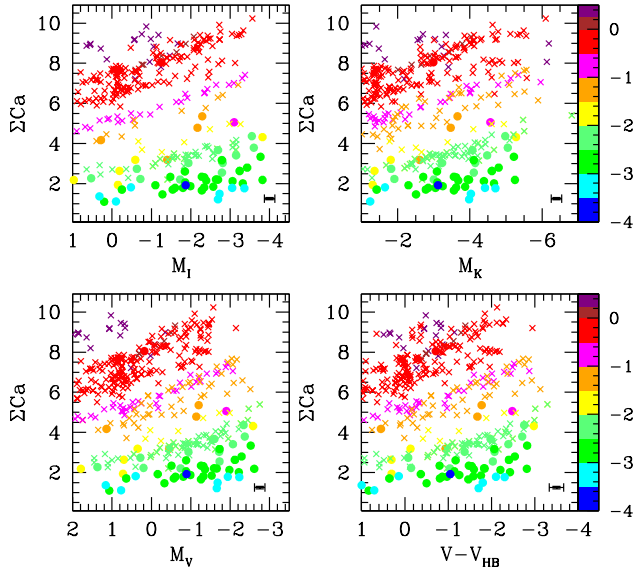


**Figure 10.** As Fig. 5 but the colors are defined as a function of  $[\text{Ca}/\text{H}]$  abundances.

(2010) solved the saturation problem at metal-poor metallicities. Although they adopted a correction procedure to account for the contribution of the damping wings of strong metal-rich to their single Gaussian fit, their calibration fails at metal-rich regimes. The calibration obtained in this paper seems to behave well in the whole range of metallicities covered.

In the left panel Figure 9 we have directly compared the metallicities calculated with the calibrations obtained in Paper I and in this paper. In general both calibrations produce similar metallicities within the uncertainties for  $-2 \leq [\text{Fe}/\text{H}] \leq 0$ . As expected, the calibration derived in paper I produces more metal-rich values for  $[\text{Fe}/\text{H}] < -2$ . This difference can be as large as 1 dex for  $[\text{Fe}/\text{H}] < -2.5$ . We perform the same comparison in right panel of Figure 9 with the metallicities computed from the calibration obtained by Starkenburg et al. (2010) from synthetic spectra. In general, there is a good agreement within the uncertainties between both calibrations for  $-3 \leq [\text{Fe}/\text{H}] \leq -0.5$ . There are differences larger than 0.5 between the values obtained from both calibrations for metallicities more metal-rich than  $[\text{Fe}/\text{H}] \sim 0$ . Again this is explained because their method do not sample properly the large wings of strong metal-rich lines. There are also large differences in the most metal-poor metallicities which may be explained by the difficulty of properly modelled the CaT lines at these extremely metal-poor metallicities.

### 6.3 Dependence of the CaT lines with Ca abundances

In spite that the strength of the CaT lines is expected to depend mainly on the Ca abundances rather than on the iron ones this is not the case, as it has been pointed by several investigations (e.g. Idiart et al. 1997; Battaglia et al. 2008). In fact, by comparing the Ca and Fe abundances determined from high-resolution spectroscopy and the CaT strength in medium-resolution spectra, Battaglia et al. (2008) found

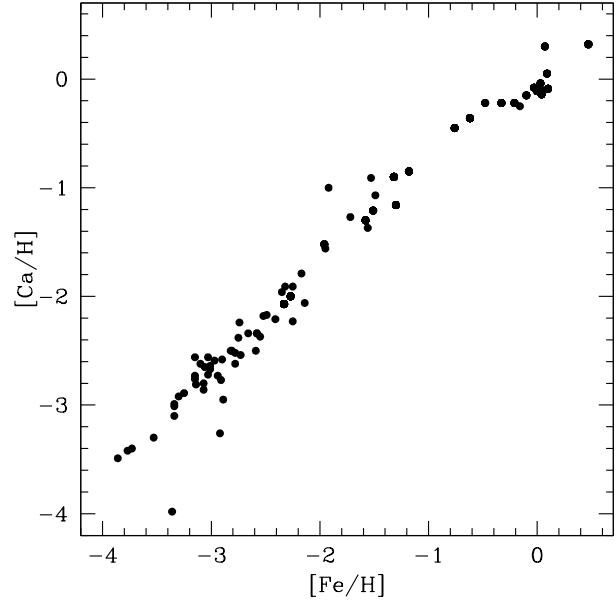


**Figure 11.** Run of  $[\text{Ca}/\text{H}]$  versus  $[\text{Fe}/\text{H}]$  for the stars in our sample, down to the very low metallicities studied in this paper.

that the CaT lines are a more robust estimator of  $[\text{Fe}/\text{H}]$  than of  $[\text{Ca}/\text{H}]$ . Starkenburg et al. (2010) found that part of this discrepancy can be reduced if non-local thermodynamic equilibrium is taken into account to derive the calcium abundances from Ca I lines. They suggest that the remaining discrepancy may relate to the outer atmospheric layers that are not very well modelled even in non-local thermodynamic equilibrium. In this section we investigate whether the same behavior holds at the very low metallicity interval.

As in Fig. 5, in Fig. 10 we have plotted the run of  $\Sigma \text{Ca}$  as a function of the different luminosity indicators used. In this case, the different colors denote different  $[\text{Ca}/\text{H}]$  ratios. As in the case of Fe, there is a clear trend with Ca abundances, as expected, since  $[\text{Fe}/\text{H}]$  is correlated with  $[\text{Ca}/\text{H}]$ , down to very low metallicities, as shown in Fig. 11. However, comparison of Fig. 5 and 10, reveals that  $\Sigma \text{Ca}$  reflects more cleanly the Fe abundances than the Ca ones. As in Paper I, we conclude that to properly investigate the relation of the CaT equivalent widths with the Ca and Fe abundances, it may be necessary to sample objects with very different  $[\text{Ca}/\text{H}]$  ratios at a given  $[\text{Fe}/\text{H}]$ .

## 7 SUMMARY

The cluster sample used in Paper I has been complemented with observations of extremely metal-poor field stars in order to obtain a new calibration of the strength of the infrared CaT lines as metallicity indicator. The obtained calibration is of very general use and applicability since: i) it is valid in the range  $-4 \leq [\text{Fe}/\text{H}] \leq +0.5$ , which is the widest metallicity range in which the behavior of the CaT lines has been homogeneously investigated. ii) it has been obtained on the basis of the traditional luminosity indicators  $V-V_{\text{HB}}$ ,  $M_V$ ,  $M_I$ , but also as a function of  $M_K$ . This will allow to use also the magnitudes derived by 2MASS, which covers al-

most the whole celestial sphere. iii) it is valid for at least five magnitudes below the tip of the RGB. iv) the contribution of each line to the global CaT index, obtained as  $\Sigma Ca = W_{8498} + W_{8542} + W_{8662}$  has been determined. The strength of each line at 8498, 8542, and 8662 Å contribute with the 19%, 47%, and 34% to  $\Sigma Ca$ , respectively.

The calibration obtained in this paper results in a tight correlation between [Fe/H] abundances measured from high resolution spectra and [Fe/H] values derived from the CaT, over the whole metallicity range covered. Former saturations of the index, at low and high metallicities, which hampered the use of the CaT in these metallicity regimes, are no longer observed. We conclude, therefore, that the CaT remains a powerful metallicity indicator, applicable to nearby extragalactic star clusters and galaxies where high resolution metallicity measurements are not possible due to the faintness of the targets.

## ACKNOWLEDGMENTS

We acknowledge the anonymous referee for comments and suggestions which have significantly improved the analysis and results presented in this paper. R.C. acknowledges funds provided by the Spanish Ministry of Science and Innovation under the Juan de la Cierva fellowship and under the Plan Nacional de Investigación Científica, Desarrollo, e Investigación Tecnológica, AYA2010-16717. This research has made use of the WEBDA database, operated at the Institute for Astronomy of the University of Vienna, and the SIMBAD database, operated at CDS, Strasbourg, France

## REFERENCES

- Andrievsky, S. M., Spite, F., Korotin, S. A., et al. 2011, A&A, 530, A105
- Armandroff, T. E., & Da Costa, G. S. 1991, AJ, 101, 1329
- Armandroff, T. E., & Zinn, R. 1988, AJ, 96, 92
- Battaglia, G., Irwin, M., Tolstoy, E., et al. 2008, MNRAS, 383, 183
- Battaglia, G., Tolstoy, E., Helmi, A., et al. 2011, MNRAS, 411, 1013
- Bragaglia, A., Carretta, E., Gratton, R. G., et al. 2001, AJ, 121, 327
- Bragaglia, A., Gratton, R. G., Carretta, E., D’Orazi, V., Sneider, C., Lucatello, S., 2012, A&A, 548, A122
- Bragaglia, A., & Tosi, M. 2003, MNRAS, 343, 306
- Bragaglia, A., Tosi, M., Andreuzzi, G., & Marconi, G. 2006, MNRAS, 368, 1971
- Breddels, M. A., et al., 2010, A&A, 511, A90
- Barklem, P. S., Christlieb, N., Beers, T. C., et al. 2005, A&A, 439, 129
- Carraro, G., Hassan, S. M., Ortolani, S., & Vallenari, A. 2001, A&A, 372, 879
- Carretta, E., Bragaglia, A., Gratton, R., D’Orazi, V., & Lucatello, S. 2009, A&A, 508, 695 (CBGDL09)
- Carretta, E., et al., 2009, A&A, 505, 117
- Carretta, E., Bragaglia, A., Gratton, R. G., et al. 2010, A&A, 520, A95
- Carretta, E., Bragaglia, A., Gratton, R., et al. 2010b, ApJ, 712, L21
- Carretta, E., Bragaglia, A., & Gratton, R. G. 2007, A&A, 473, 129
- Carretta, E., Cohen, J. G., Gratton, R. G., & Behr, B. B. 2001, AJ, 122, 1469
- Carretta, E., & Gratton, R. G. 1997, A&AS, 121, 95 (CG97)
- Carretta, E., Gratton, R. G., Bragaglia, A., Bonifacio, P., & Pasquini, L. 2004, A&A, 416, 925
- Carretta, E., Lucatello, S., Gratton, R. G., Bragaglia, A., & D’Orazi, V. 2011, A&A, 533, A69
- Carrera, R. 2012, A&A, 544, A109
- Carrera, R., Gallart, C., Hardy, E., Aparicio, A., & Zinn, R. 2008a, AJ, 135, 836
- Carrera, R., Gallart, C., Aparicio, A., et al. 2008b, AJ, 136, 1039
- Carrera, R., Gallart, C., Aparicio, A., & Hardy, E. 2011, AJ, 142, 61
- Carrera, R., Gallart, C., Pancino, E., & Zinn, R. 2007, AJ, 134, 1298 (Paper I)
- Carrera, R., & Pancino, E. 2011, A&A, 535, A30
- Catelan, M., & Cortés, C. 2008, ApJ, 676, L135
- Cayrel, R., Depagne, E., Spite, M., et al. 2004, A&A, 416, 1117
- Cenarro, A. J., Cardiel, N., Gorgas, J., et al. 2001, MNRAS, 326, 959
- Cole, A. A., Smecker-Hane, T. A., Tolstoy, E., Bosler, T. L., & Gallagher, J. S. 2004, MNRAS, 347, 367
- Cole, A. A., Tolstoy, E., Gallagher, J. S., III, & Smecker-Hane, T. A. 2005, AJ, 129, 1465
- Da Costa, G. S., Hatzidimitriou, D., 1998, AJ, 115, 1934
- Demarque, P., Woo, J.-H., Kim, Y.-C., & Yi, S. K. 2004, ApJS, 155, 667
- Diaz, A. I., Terlevich, E., & Terlevich, R. 1989, MNRAS, 239, 325
- Feltzing, S., & Johnson, R. A. 2002, A&A, 385, 67
- Feltzing, S., Primas, F., & Johnson, R. A. 2009, A&A, 493, 913
- Friel, E. D., Jacobson, H. R., & Pilachowski, C. A. 2010, AJ, 139, 1942
- Friel, E. D., Jacobson, H. R., & Pilachowski, C. A. 2005, AJ, 129, 2725
- Friel, E. D., Janes, K. A., Tavaréz, M., et al. 2002, AJ, 124, 2693
- Fullton, L. K. 1996, PASP, 108, 545
- Fulbright, J. P. 2000, AJ, 120, 1841
- Gim, M., Vandenberg, D. A., Stetson, P. B., Hesser, J. E., & Zurek, D. R. 1998, PASP, 110, 1318
- Giridhar, S., Lambert, D. L., Gonzalez, G., Pandey, G., 2001, PASP, 113, 519
- Gonzalez, G., & Wallerstein, G. 2000, PASP, 112, 1081
- Harris, W. E. 1996, AJ, 112, 1487
- Helmi, A., Irwin, M. J., Tolstoy, E., et al. 2006, ApJ, 651, L121
- Idiart, T. P., Thévenin, F., & de Freitas Pacheco, J. A. 1997, AJ, 113, 1066
- Hollek, J. K., Frebel, A., Roederer, I. U., et al. 2011, ApJ, 742, 54
- Jacobson, H. R., Friel, E. D., & Pilachowski, C. A. 2009, AJ, 137, 4753
- Jacobson, H. R., Pilachowski, C. A., & Friel, E. D. 2011, AJ, 142, 59
- Johnson, J. A. 2002, ApJS, 139, 219

- Jones, J. E., Alloin, D. M., & Jones, B. J. T. 1984, *ApJ*, 283, 457
- Jorgensen, U. G., Carlsson, M., & Johnson, H. R. 1992, *A&A*, 254, 258
- Kassis, M., Janes, K. A., Friel, E. D., & Phelps, R. L. 1997, *AJ*, 113, 1723
- Kraft, R. P., & Ivans, I. I. 2003, *PASP*, 115, 143
- Lai, D. K., Bolte, M., Johnson, J. A., et al. 2008, *ApJ*, 681, 1524
- Lianou, S., Grebel, E. K., & Koch, A. 2011, *A&A*, 531, A152
- Luck R. E., Bond H. E., 1985, *ApJ*, 292, 559
- McWilliam A., 1990, *ApJS*, 74, 1075
- McWilliam, A., Geisler, D., & Rich, R. M. 1992, *PASP*, 104, 1193
- McWilliam A., Preston G. W., Sneden C., Searle L., 1995, *AJ*, 109, 2757
- Monelli M., et al., 2013, *MNRAS*, 1005
- Norris J. E., Gilmore G., Wyse R. F. G., Wilkinson M. I., Belokurov V., Evans N. W., Zucker D. B., 2008, *ApJ*, 689, L113
- Olszewski, E. W., Schommer, R. A., Suntzeff, N. B., & Harris, H. C. 1991, *AJ*, 101, 515
- Ortolani, S., Bica, E., & Barbuy, B. 1992, *A&As*, 92, 441
- Pancino, E., Carrera, R., Rossetti, E., & Gallart, C. 2010, *A&A*, 511, A56
- Parisi, M. C., Geisler, D., Grocholski, A. J., Clariá, J. J., & Sarajedini, A. 2010, *AJ*, 139, 1168
- Pilachowski, C. A., Sneden, C., & Kraft, R. P. 1996, *AJ*, 111, 1689
- Pont, F., Zinn, R., Gallart, C., Hardy, E., & Winnick, R. 2004, *AJ*, 127, 840
- Rosenberg, A., Saviane, I., Piotto, G., & Aparicio, A. 1999, *AJ*, 118, 2306
- Rosvick, J. M., & Vandenberg, D. A. 1998, *AJ*, 115, 1516
- Rutledge, G. A., Hesser, J. E., Stetson, P. B., et al. 1997, *PASP*, 109, 883
- Rutledge, G. A., Hesser, J. E., & Stetson, P. B. 1997, *PASP*, 109, 907
- Salaris, M., Weiss, A., & Percival, S. M. 2004, *A&A*, 414, 163
- Salaris, M., & Weiss, A. 2002, *A&A*, 388, 492
- Sarajedini, A., von Hippel, T., Kozhurina-Platais, V., & Demarque, P. 1999, *AJ*, 118, 2894
- Saviane, I., da Costa, G. S., Held, E. V., et al. 2012, *A&A*, 540, A27
- Sestito, P., Bragaglia, A., Randich, S., et al. 2008, *A&A*, 488, 943
- Shetrone, M. D., & Keane, M. J. 2000, *AJ*, 119, 840
- Skrutskie, M. F., Cutri, R. M., Stiening, R., et al. 2006, *AJ*, 131, 1163
- Starkenburg, E., Hill, V., Tolstoy, E., et al. 2010, *A&A*, 513, A34
- Stetson, P. B., Bruntt, H., & Grundahl, F. 2003, *PASP*, 115, 413
- Suntzeff, N. B., Mateo, M., Terndrup, D. M., et al. 1993, *ApJ*, 418, 208
- Suntzeff, N. B., Schommer, R. A., Olszewski, E. W., & Walker, A. R. 1992, *AJ*, 104, 1743
- Sung, H., Bessell, M. S., Lee, H.-W., Kang, Y. H., & Lee, S.-W. 1999, *MNRAS*, 310, 982
- Tautvaišienė, G., Edvardsson, B., Puzeras, E., & Ilyin, I. 2005, *A&A*, 431, 933
- Tolstoy, E., Irwin, M. J., Cole, A. A., et al. 2001, *MNRAS*, 327, 918
- Warren, S. R., & Cole, A. A. 2009, *MNRAS*, 393, 272
- Wu Y., Singh H. P., Prugniel P., Gupta R., Koleva M., 2011, *A&A*, 525, A71
- Yong, D., Carney, B. W., & Teixeira de Almeida, M. L. 2005, *AJ*, 130, 597
- Zhang, L., Ishigaki, M., Aoki, W., Zhao, G., & Chiba, M. 2009, *ApJ*, 706, 1095
- Zinn, R., & West, M. J. 1984, *ApJS*, 55, 45
- Zwitter T., et al., 2010, *A&A*, 522, A54

This paper has been typeset from a  $\text{\LaTeX}$  file prepared by the author.